Strain-Dependent Cross-Bridge Cycle for Muscle II. Steady-State Behavior

D. A. Smith and M. A. Geeves
Max-Planck Institute for Molecular Physiology, 44026 Dortmund, Germany

ABSTRACT Quantitative predictions of steady-state muscle properties from the strain-dependent cross-bridge for muscle are presented. With a stiffness of 5.4×10^{-4} N/m per head, a throw distance of 11 nm, and three allowed actin sites/head, isometric properties and their dependence on phosphate and nucleotide levels are well described if the tension-generating step occurs before phosphate release. At very low ATP levels, rigorlike states with negative strain are predicted. The rate-limiting step for cycling and ATP consumption is strain-blocked ADP release for isometric and slowly shortening muscle. Under rapid shortening, ATP hydrolysis on detached heads is the rate-limiting step, and the ratio of bound ATP to bound ADP.Pi increases by a factor of 7. At large positive strains, bound heads must be forcibly detached from actin to account for tension in rapid extension, but forced detachment in shortening has no effect without destroying isometric attached states. Strain-blocked phosphate release as proposed produces modest inhibition of the ATPase rate under rapid shortening, sufficient to give a maximum for one actin site per helix turn. Alternative cross-bridge models are discussed in the light of these predictions.

INTRODUCTION

The three-line model of Geeves et al. (1984), with strain-dependent transitions determined by structural assumptions and transition-state theory (see the companion paper, Smith and Geeves, 1995), is tested against basic steady-state properties of fast muscle at full activation. The aim is to understand how the model can be made to reproduce these properties, using only a few parameters in addition to the rate constants of the solution cycle. Attention is focused on the effects of blocking the ADP release and ATP binding steps at positive strains and also on phosphate release (and binding) at negative strains, as suggested in the companion paper. The validity of so-called tightly coupled models of the cross-bridge cycle, in which heads must hydrolyze one molecule of ATP per cycle of attachment and detachment, is assessed by introducing forced detachment at both large positive and negative strains. For simplicity, comparisons with experiment are restricted to one muscle type at one temperature (rabbit psoas at 20°C), which may not represent the whole range of behavior shown even by fast muscle fibers.

Cross-bridge modeling is not made easier by working with the full set of states in the 3G model of Geeves et al. (1984). Although many strain-free rate constants are required, their values are tightly constrained by solution-kinetic measurements and by detailed balancing around the eight internal loops (Fig. 1, companion paper). Also, many rates of ligand binding/dissociation for detached and rotated states are slow enough to have negligible effect on the operation of the cycle for fully activated muscle. However, our approach to modeling is to allow all transitions observed in solution as represented by the 3G scheme and to let the model itself determine which states are occupied under a wide variety of conditions. This approach permits very little adjustment of strain-free rate constants, with the exception of S1 binding rates to actin as discussed previously.

The model is further constrained by the use of transition-state theory to predict the strain-dependence of the same reactions in fibers. In its simplest form (see the companion paper) only five additional parameters are needed to specify the entire model at sarcomere level: the cross-bridge stiffness k, the throw distance $2h$, the number of actin sites available to each S1 head, and the displacements Δ_D and Δ_P required for ADP release/ATP binding and Pi release. Acceptable behavior is produced only in a very small region of this five-dimensional parameter space, k and h were kept fixed throughout most of these calculations. With $2h = 11$ nm (two length units) and $k = 5.35 \times 10^{-4}$ N/m, $kh = 2.94$ pN is the unit of tension, and the ratio of strain energy to elastic energy is $kh^2/RT = 4.0$. Hence the force generated from one throw of a single head is 5.88 pN, which is in the range observed recently by Finer et al. (1994) using a laser-trapped actin filament. Definitions of mathematical symbols used in this paper appear in Table 1 of the companion paper.

MATHEMATICAL AND COMPUTATIONAL METHODS

The mathematical formulation of the sliding filament model is given in terms of state probabilities $p_{il}(x, t)$ for whatever S1 head has its central actin site displaced by distance x at time t (the Eulerian formulation). In this model i runs from 0 to 11, as there are 12 chemically distinct states. Inasmuch as their probabilities sum to unity, it is convenient to omit state 0 (chosen as M.T) from the list. The three remaining

Received for publication 24 October 1994 and in final form 15 May 1995.
Address reprint requests to Dr. David Smith, The Randall Institute, King's College London, 26-29 Drury Lane, London WC2B 5RL, UK. Tel.: 71-836-8851; Fax: 71-497-9078; E-mail: dave@muscle.rai.kcl.ac.uk.

0006-3495/95/08/538/15 $2.00

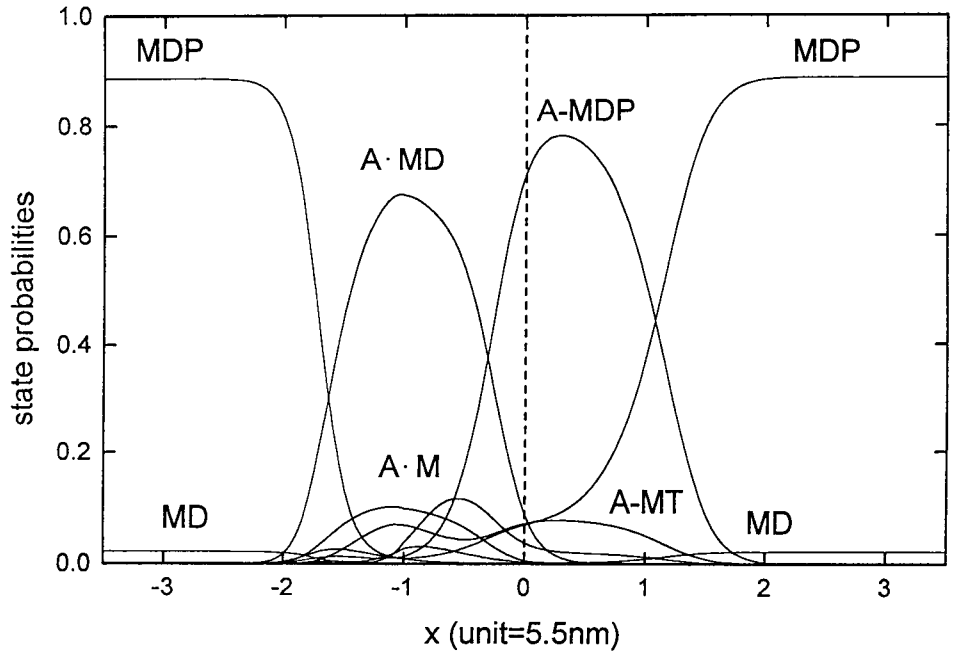

FIGURE 1 Calculated steady-state properties for the isometric condition and standard parameter values (Table 1, companion paper), with $L = 0$ (one actin site/head).

detached states are labeled by $i = 1, 2, 3$, leaving eight bound states. For these states the actin site must also be specified by the site index l, which is taken to run from $-L$ to $+L$, where L can be chosen $=0$, 1, or 2. The cross-bridge strain to site l is therefore $y = x + lc$, where c is the spacing between actin sites measured down the filaments. As c is 5.5 nm, it is convenient to use this as a unit of length, which allows the throw distance to be varied. Usually h is set equal to one unit of this length scale. The state probabilities satisfy rate equations that in the presence of filament motion are

$$\frac{\partial p_i(x,t)}{\partial t} - v(t)\frac{\partial p_i(x,t)}{\partial x} = \sum_{j=0}^{3}\{k_{ji}(x)p_j(x,t) - k_{ij}(x)p_i(x,t)\} \quad (1a)$$

$$+ \sum_{l=-L}^{L}\sum_{j=4}^{11}\{k_{ji}(x+lc)p_{jl}(x,t) - k_{ij}(x+lc)p_i(x,t)\}$$

for $i = 1$–3 and

$$\frac{\partial p_{il}(x,t)}{\partial t} - v(t)\frac{\partial p_{il}(x,t)}{\partial x} = \sum_{j=0}^{3}\{k_{ji}(x+lc)p_j(x,t) - k_{ij}(x+lc)p_{il}(x,t)\} \quad (1b)$$

$$+ \sum_{j=4}^{11}\{k_{ji}(x+lc)p_{jl}(x,t) - k_{ij}(x+lc)p_{il}(x,t)\}$$

for $i = 4$–11, where $v(t)$ is shortening velocity per half-sarcomere at time t. The left-hand side is the derivative following the motion. In this Eulerian formulation attention is focused on whatever head has a given value of strain x at time t, even though the x value of a given head varies with time at a rate $-v$. Because of the vernier effect induced by different thick and thin filament periodicities, tension, stiffness, and ATPase rates are calculated as averages over all x values that fill one half-pitch of the actin helix, i.e., $-b/2$ to $b/2$, or -3.5 to 3.5 because $b = 38.5$ nm $= 7$ units of the length scale. For example, average tension per head T is given by

$$T(t) = \frac{1}{b}\sum_{i=4}^{11}\sum_{l=-L}^{L}\int_{-b/2}^{b/2} t_i(x+lc)p_{il}(x,t)\mathrm{d}x, \quad (2)$$

where $t_i(x) = \mathrm{k}x$ for attached states ($i = 4, 7$) or $\mathrm{k}(x + 2h)$ for rotated states ($i = 8, 11$). Tension is calculated in units of $\mathrm{k}h$, where k is stiffness per cross-bridge.

The ATPase rate per head R is usually calculated as the rate of hydrolysis of ATP on myosin, detached, attached, or rotated. Under steady-state conditions this quantity is equal to the net left-to-right flux across the cross-bridge cycle and can therefore be calculated equivalently as the net rate of phosphate or ADP release, the rate of ATP binding, or the rate of ATP cleavage (the hydrolysis step). Only steady-state conditions are considered in this paper, but all four quantities were calculated. Under isometric conditions they were equal to the computed accuracy (double precision arithmetic).

For computation, Eqs. 1 should be rearranged by packaging the state probabilities into a single column vector $\mathbf{p}(x, t)$ of $N_M = 3 + 8(2L + 1)$ entries, and the rate constants into a square matrix of the same size. The largest matrices required are therefore 43×43 if $L = 2$, but most calcula-

tions were done with $L = 0$ and $L = 1$. The final form of these equations is

$$\frac{\partial \mathbf{p}(x, t)}{\partial t} - v\frac{\partial \mathbf{p}(x, t)}{\partial x} = \mathbf{f}(x) - M(x)\mathbf{p}(x, t), \quad (3)$$

where the column vector $\mathbf{f}(x)$ and the matrix $M(x)$ are determined by the rate constants $k_{ij}(x + lc)$ for $i, j = 0, \ldots, 11$ and $l = -L, \ldots, L$. However, the state probabilities were reduced for graphical purposes to a column vector of order 11 by summing them over all actin sites ($l = -L, \ldots, L$) with the same strain $y = x + lc$.

Isometric properties are calculated by setting the right-hand side of Eq. 3 to zero and solving for the time-independent $\mathbf{p}(x)$. This procedure can be computationally hazardous for $L > 0$ because of the huge variation in rate constants with strain over the full range of x values. These problems were cured by imposing a lower cutoff at $x = -3.5$, interpreted as a lower limit for elastic behavior as described. If necessary, one can use the time-dependent equation with $v = 0$ and allow a steady state to evolve.

Behavior under steady shortening or extension was calculated by using the backward Euler method, which is stable under all step sizes in x but requires inversion of a matrix related to $M(x)$ at each step. The step size was normally 0.025 unit. The overall accuracy in tension is usually 1–2%, as established by test runs with step sizes of 0.01 and 0.005. In shortening or extending muscle, the boundary conditions on $\mathbf{p}(x, t)$ at $x = \pm b/2$ are very important. We used periodic boundary conditions on detached states only. Technically, the usual form of the sliding filament model is invalid if there is a finite probability of bound states at both boundaries, because in that case adjacent heads spaced by 43 nm would be competing for the same set of actin sites and the assumption of independently binding heads would be invalid. The state distribution diagram should be used to check that bound states are absent at both boundaries, which can usually be done by shifting the entire x range. When this is achieved, periodic boundary conditions on bound states are unnecessary. Equality of the ATPase rates calculated by the four methods given above is a sensitive test for the localization of bound states within the allowed range, which is often difficult to achieve without some forced detachment at negative strains.

Rate constants in the form k_{ij} refer to numerically labeled states, not to the subscript–superscript scheme in Table 1 of the companion paper. Numeric labels are as follows: 0 = MT, 1 = M, 2 = MD, 3 = MDP, 4 = A-MDP, 5 = A-MD, 6 = A-M, 7 = A-MT, 8 = A.MDP, 9 = A.MD, 10 = A. M, and 11 = A.MT. All calculations were made with three actin sites/head ($L = 1$) unless stated otherwise.

ISOMETRIC BEHAVIOR

Standard values for the biochemical and structural parameters of the 3G model are given in Table 1 of the companion paper and are used throughout unless stated otherwise. These are notional values for rabbit psoas muscle at 20°C. The displacement barrier for strain-blocked ADP release and ATP binding was $\Delta_D = 4.125$ nm (0.75 unit), which determines a lower limit of -2.375 in x for the strain-blocked region. Strain blocking of phosphate release at negative strains has no effect on isometric properties and was not used in this section. All quantities were calculated for one and three allowed actin sites per head ($L = 0, 1$). Elastic cutoffs were not used for isometric properties, except that d_- was set at -3.5 to avoid numerical problems with the inversion of the reaction matrix for $L > 0$.

Table 1 lists isometric tension, high-frequency stiffness (expressed as the fraction of heads bound to actin), and ATPase rate per head calculated from the standard parameter set. For convenience, the unloaded contraction velocity is also listed. The columns headed by superscripted values of R give ATPase contributions from fluxes through ATP cleavage in detached, attached, and rotated states.

Expected values for isometric tension are 1–3 pN per head, with some uncertainty arising from estimated densities of myosin heads per sarcomere. The calculated stiffness varies from 35% of all heads bound for one allowed actin site, 70% for three sites, and over 90% for five. The last choice seems unrealistic, as calculated tension and ATPase actually decrease, as the result of binding over the whole range of strain values. It appears that three sites ($L = 1$) may

TABLE 1 Isometric predictions and unloaded contraction velocity

α	h	Δ_D	No. Actin Sites	T (pN)	κ	R	$R^{(0)}$	$R^{(1)}$	$R^{(2)}$	v_0 (μm/s)
4	1.0	0.75	1	0.623	0.353	3.04	2.56	0.45	0.03	2.19
			3	1.170	0.630	4.96	2.85	2.07	0.04	2.42
6	1.0	0.75	1	0.710	0.316	0.58	0.53	0.05	0.01	1.81
			3	1.530	0.593	1.03	0.60	0.42	0.01	2.06
4	1.5	0.75	1	0.997	0.485	8.25	6.41	1.78	0.06	—
			3	1.552	0.757	11.2	5.82	5.32	0.08	—
4	1.0	1.125	1	0.776	0.388	0.91	0.83	0.07	0.01	1.80
			3	1.488	0.671	1.25	0.87	0.37	0.01	1.22

Columns 5–12: Isometric tension T per head, stiffness κ (fraction of heads bound), rate R of ATP cleavage (in s^{-1}/head), and the detached, attached, and rotated contributions $R^{(i)}$ ($i = 0, 1, 2$), also unloaded contraction velocity, calculated for values of Table 1 of the companion paper. Standard values of α, h, and Δ_D are used in the top two rows. Rows below show the effects of increasing each in turn by 50%. For $h = 1.5$, unloaded contraction velocities are large but cannot be legitimately calculated within the allowed range of x values.

be optimal. Unloaded contraction velocities of 2.5 (μm/s)/half-sarcomere are typical for fast-twitch fibers (e.g., see Edman, 1979).

The predicted ATP hydrolysis rate of 5.0 s^{-1} with three sites is between those observed for fibers and myofibrils at 20°C (Ferenczi et al., 1984b; Herrmann et al., 1994). It is controlled by strain-blocked ADP release through the value of Δ_D and by the rate constants for ATP hydrolysis on detached heads (100 s^{-1}) and bound heads (50 s^{-1}). Introducing a lower limit for elastic behavior will cause some reduction in isometric ATPase but only for $d_- > -2$. Almost no hydrolysis takes place via the rotated state A.MT, which is on a rapid escape path. The rate of cleavage of ATP via attached (A) states is sensitive to the number of actin sites and is very small for one actin site ($L = 0$).

Table 1 also shows the effects of increasing cross-bridge stiffness, h and Δ_D by 50% in turn. Despite appearances, these changes are generally undesirable. A larger stiffness precludes the proper simulation of tension responses to length steps (Huxley and Simmons, 1971) and to AC stiffness measurements also, and a throw distance much above 11 nm is unlikely on structural grounds. More effective strain blocking does produce more isometric tension at less ATPase cost but reduces the unloaded contraction velocity.

The strain-dependent populations of cross-bridge states are shown in Fig. 1, which uses one actin site for clarity of illustration. The dominant bound states are the attached state A-MDP and the rotated state A.MD. Tension is kx from attached states and k($x + 2h$) for rotated ones. With this in mind, most isometric properties of this model can be understood in terms of the three parameters x_+, x_* and x_-, which mark the boundaries of the attached and rotated distributions against strain, as discussed in the companion paper. The first two can be calculated from Eq. 9 of that paper, using first-order equilibrium constants $K_1^{(DP)} = 10$ (for an effective actin concentration of 1 mM), $K_2^{(DP)} = 1$, and $K_P^{(2)} = 1000$ at 1-mM phosphate from Table 1 of the companion paper. Hence $x_+ = 1.07$ and $x_* = -0.14$, in reasonable agreement with the right- and left-hand edges of the distribution of A-MDP states. The slightly negative value of the latter means that only a few attached states generate negative tension. The left-hand edge of the distribution of the dominant rotated state A.MD is above -2.0, so all rotated states generate positive tension. Equation A8 of the Appendix predicts that $x_- = -1.7$. The rigor state A.M also carries some tension, but A.MDP is barely populated because the rate of phosphate release $k_P^{(2)}$ is not strain blocked and was set at 1000 s^{-1}. Lower values have been assigned from caged phosphate release experiments (Millar and Homsher, 1990) but will create difficulties in achieving high unloaded contraction velocities in the present model. The rate observed by Millar and Homsher may have been partially strain blocked by the mechanism suggested in the companion paper.

To summarize: for activated isometric muscle the dominant bound states of the 3G model are the attached A-MDP state and the rotated A.MD state, as expected. The parameters determining the boundaries of these states against strain are as predicted from simple equilibrium and kinetic ideas and are close to optimum for achieving maximum isometric tension. More tension and stiffness can be generated by allowing more actin sites/head, by raising first-order S1 binding constants (e.g., the effective actin concentration could be above 1 mM), or by increased strain control of ADP release. The first two changes would increase the isometric ATPase, but the last would decrease it.

Dependence on ATP and ADP

Experimentally, isometric tension is found to be a slightly decreasing function of ATP level above 50–100 μM or so (Ferenczi et al., 1982; Cooke and Bialek, 1979), while increasing the ADP level at a fixed millimolar level of ATP produces a similar increase (Cooke and Pate 1985). Both effects saturate at high levels of nucleotide. At 10°C, the fall in tension with increasing ATP flattens out above 0.5 mM, and the rise with increasing ADP also saturates above 2 mM or so. The total changes in tension produced in this way are of the order of 20–30%. Thus ATP/ADP competitively inhibit/effect the occupancy of the tension-generating A.MD state, which works because ADP release is reversible.

These results can be viewed as indirect evidence for strain control of ADP release, at least in the context of the 3G model with its single A.MD state; otherwise this state would not be populated for positive strains ($x > -2h$). If the cleft opens by the same amount for ADP release and ATP binding, then both processes would be controlled by strain in the same way if, as suggested in the companion paper, strain inhibits the opening of the nucleotide cleft. This could be tested through the dependence of tension or ATPase rate on nucleotide concentrations. The effective rate constants for the combined process of D release and T binding can be calculated by Michaelis–Menten (M-M) kinetics, provided that the population of the rigor state A.M remains negligible. This calculation predicts that the effective rate constants vary with nucleotide levels only through the ratio $[T]/[D]$, and that the M-M constants for ATP binding and ADP release, as seen in isometric tension, are $C[D]$ and $[T]/C$, where

$$C = \tilde{k}_{-D}/\tilde{k}_T \tag{4}$$

and the superscript implies second-order rate constants. For the values of Table 1 of the companion paper, $C = 4$. However, this picture is too simple. The computed dependence of tension on ADP level shows a significant effect only if the rigor state is populated. This can be done if the parameter Δ_D for strain-blocked ADP release is not too large. Similarly, excess millimolar ATP causes a drop in tension only if the second-order rate constant for ATP binding to the rigor state is not too large. More accurate expressions for the Michaelis–Menten constants are derived in the Appendix (Eqn. A10).

Figs. 2 *A–C* show the computed effects of ATP on tension, ATPase, and unloaded contraction velocity v_0 for the standard parameter set. The 20% drop in tension from the maximum is close to observations at 20°C (Cooke and Bialek, 1979). The model also predicts that ATPase rates fall abruptly as ATP is reduced or ADP is increased beyond levels determined by the M-M constants above: this should be tested experimentally. The unloaded contraction velocity varies as expected from the work of Cooke and Bialek (1979) and Ferenczi et al. (1984a), and our prediction is similar to that of Pate and Cooke (1989) who show that a classical M-M law is numerically obeyed. With $[D] = 30$ μM, our results are qualitatively described by such a law with a M-M constant of 1 mM (for tension), 0.4 mM for ATPase, and 0.25 mM for v_0. The M-M constant for tension is predicted from Eq. A10 at 2.9 mM, using $[D] = 30$ μM.

ADP dependences (Figs. 2 *D–F* are in the opposite sense, as expected, with notional M-M constants of 1.5 mM for tension, 4 mM for ATPase, and ~2 mM for v_0 using $[T] = 5$ mM. The rise in tension is nearly 20%, similar to that observed by Cooke and Pate (1985). To achieve this effect it is necessary to limit the rate of ATP binding, so that the rigor state is occupied and also to limit the strength of strain-blocked ADP release so that ADP binding can raise the population of A.MD states over their whole range of strain values, not just at the left-hand edge. The calculated value of the ADP M-M constant for tension is 1.6 mM at $[T] = 5$ mM. Thus ADP, and ATP above 0.1 mM, appear to act as classical inhibitors/effectors of tension, ATPase, and unloaded velocity, even although the last-named value is determined by balancing tension contributions of either sign from heads with different strains and therefore with different kinetics.

"Quasi-rigor" states are produced at submicromolar levels of ATP (Figs. 2 *A* and *B*). Their nature is revealed by the state distributions in Fig. 3, calculated for $[T] = 1$ nM and the standard value of $[D]$. The drop in tension seen in Fig. 2 *A* is caused by negatively strained A.MD states ($x < -2h$). The left-hand edge to this distribution arises from the very low rate of binding of MDP to an attached state at large compressive strains and is determined by equating the binding rate $k_1(x)$ to the unstrained rate k_T of ATP binding and subsequent dissociation of A.MT from actin. Hence this edge moves to the left as the ATP level is reduced. How-

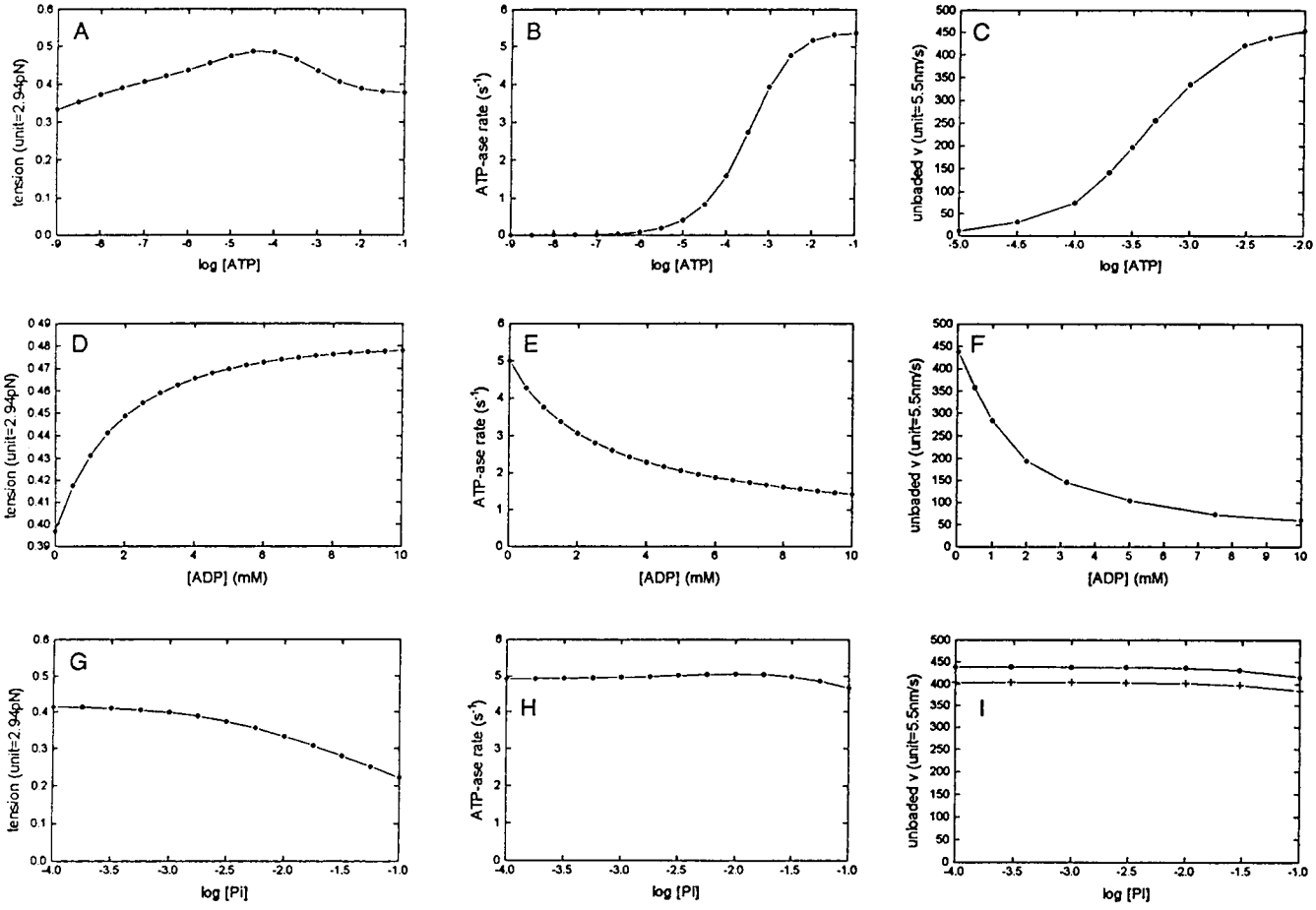

FIGURE 2 Isometric tension, ATPase and unloaded contraction velocity as a function of (*A–C*) ATP, (*D–F*) ADP, and (*G–I*) phosphate concentrations, calculated for $L = 1$ (three actin sites) and no strain blocking of phosphate release. The lower trace in *I* shows the effect of strain-blocked Pi release with $\Delta_P = 0.7$ unit.

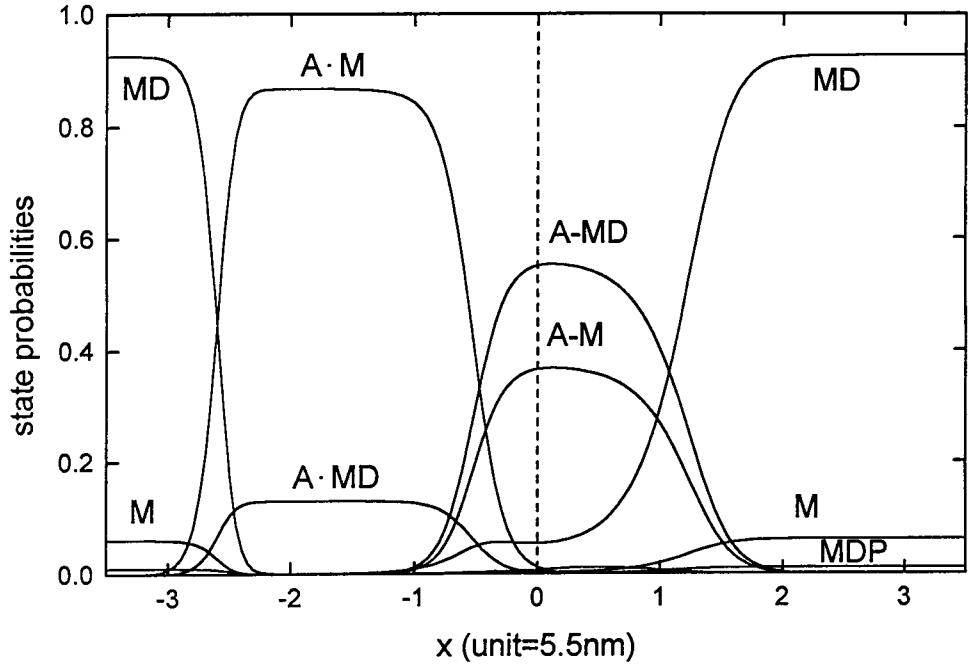

FIGURE 3 Computed steady-state probabilities for an isometric state at very low ATP concentration (1 nM) showing both positively and negatively strained rigor states (A.M). The attached states are a mixture of A-M and A-MD. Other conditions are as in Table 1 of the companion paper, and $L = 0$.

ever, the time required to establish A.MD states with such large negative strains is very large, implying that the rigor state is not unique but changes very slowly in time after formation by removal of ATP. Negatively strained rigor cross-bridges can also be produced by external procedures (Dantzig et al., 1991). Caged-ATP experiments from rigor states should probe both the existence of negatively strained rigor bridges generated without such protocols and the existence of the strain-blocking mechanism proposed here for ADP release, etc. An initial burst of ADP is expected in such experiments.

Phosphate dependence

Excess inorganic phosphate is known to reduce isometric tension in many muscles according to a logarithmic law (Cooke and Pate, 1985; Millar and Homsher, 1992). This can be understood in terms of the logarithmic dependence of x_* on phosphate concentration $[P]$, which follows from Eq. 9b of the companion paper when $K_P^{(2)} \gg 1$:

$$x_*([P]) = \text{const.} - \frac{RT}{2kh} \ln[P] \qquad ([P] \ll \tilde{K}_P^{(2)}) \quad (5)$$

(ln denotes the natural logarithm). This law arises when A and R (rotated) states (A-MDP and A.MDP+A.MD) are in rapid equilibrium. It translates into a linear dependence of tension with $\ln[P]$, as observed, if tension varies linearly with x_* and there are no other phosphate-dependent effects on tension. Our simulations (Fig. 2 *G*) lead to a logarithmic decrease of tension of the correct size for phosphate levels above 1 mM and below the 1-M dissociation constant (Table 1, companion paper). The slope of this decrease is relatively insensitive to parameter changes, as the rate of decrease of x_* with $\ln[P]$ in Eq. 5 is inversely proportional to k and h but independent of all reaction rates. Millar and Homsher find that the drop in relative tension with $\ln[P]$ is smaller for slow fibers, which would be consistent with a universal slope for absolute tension if slow fibers generate more tension than fast ones for the same phosphate level. If cross-bridge stiffness and throw distance are similar for different forms of myosin, we conclude that the dependence of absolute isometric tension on $\ln[P]$ in the allowed range should also be similar for different muscle types.

This expected dependence of tension on phosphate is not reproduced at phosphate levels below 10 mM because the rate of phosphate binding is below 10 s^{-1}, which is insufficient to put the phosphate release/binding step in rapid equilibrium as required. The binding rate cannot be raised without increasing the rate of Pi release above 1000 s^{-1}, and expected values for the equilibrium constant are, if anything, above 1 M. Thus some form of phosphate collision complex may be required for the linearity below 10 mM in Fig. 2 *G*. The introduction of collision states into the 3G model is beyond the scope of this investigation.

The phosphate dependence of the isometric ATPase rate is not known, but Fig. 2 *H* shows that no logarithmic dependence is expected. The predicted drop at 1-M phosphate is in line with a dissociation constant of this value. The same considerations apply to the unloaded contraction velocity (Fig. 2 *I*), which is known to be almost independent of phosphate levels up to 12 mM (Cooke and Pate, 1985). Thus the dependence of isometric properties on phosphate and nucleotide levels is, with one exception as discussed, satisfactorily predicted by the 3G model with existing rate and equilibrium constants, provided that only moderate strain blocking of ADP release is used.

Comparison of ATPase rates in fibers and solution

In solution, the ATP hydrolysis pathways are different from what is predicted in fibers by any model requiring a large strain dependence of its rate constants. It is not possible to make solutions with protein concentrations as high as the physiological values in Table 1 of the companion paper, but the ATPase rate can be calculated for these values as a function of actin concentration [*A*]. This has been done to illustrate the importance of strain in controlling ATPase pathways in fibers.

To achieve a rough correspondence with existing measurements at low ionic strength (Stein et al., 1979, 1981) it is necessary to lower the actin-binding rates for M.DP and MT, which are at the upper end of what is possible. For fibers, first-order binding rates are virtually unknown, because steric restrictions on S1 heads mean that the effective actin concentration is undefined and possibly above 1 mM. However, in solutions of low ionic strength the second-order binding rates are well characterized (Geeves, 1992). An approximate correspondence can be made by assigning $\bar{k}_1^{(DP)} = 2 \times 10^6\ M^{-1}\ s^{-1}$ and $\bar{k}_1^{(T)} = 1 \times 10^6\ M^{-1}\ s^{-1}$ rather than the values in Table 1, which were deliberately set near the maximum for a diffusion-controlled reaction. The binding constants in Table 1 were not adjusted.

Fig. 4 *A* shows the net ATP cleavage rate versus [*A*] and

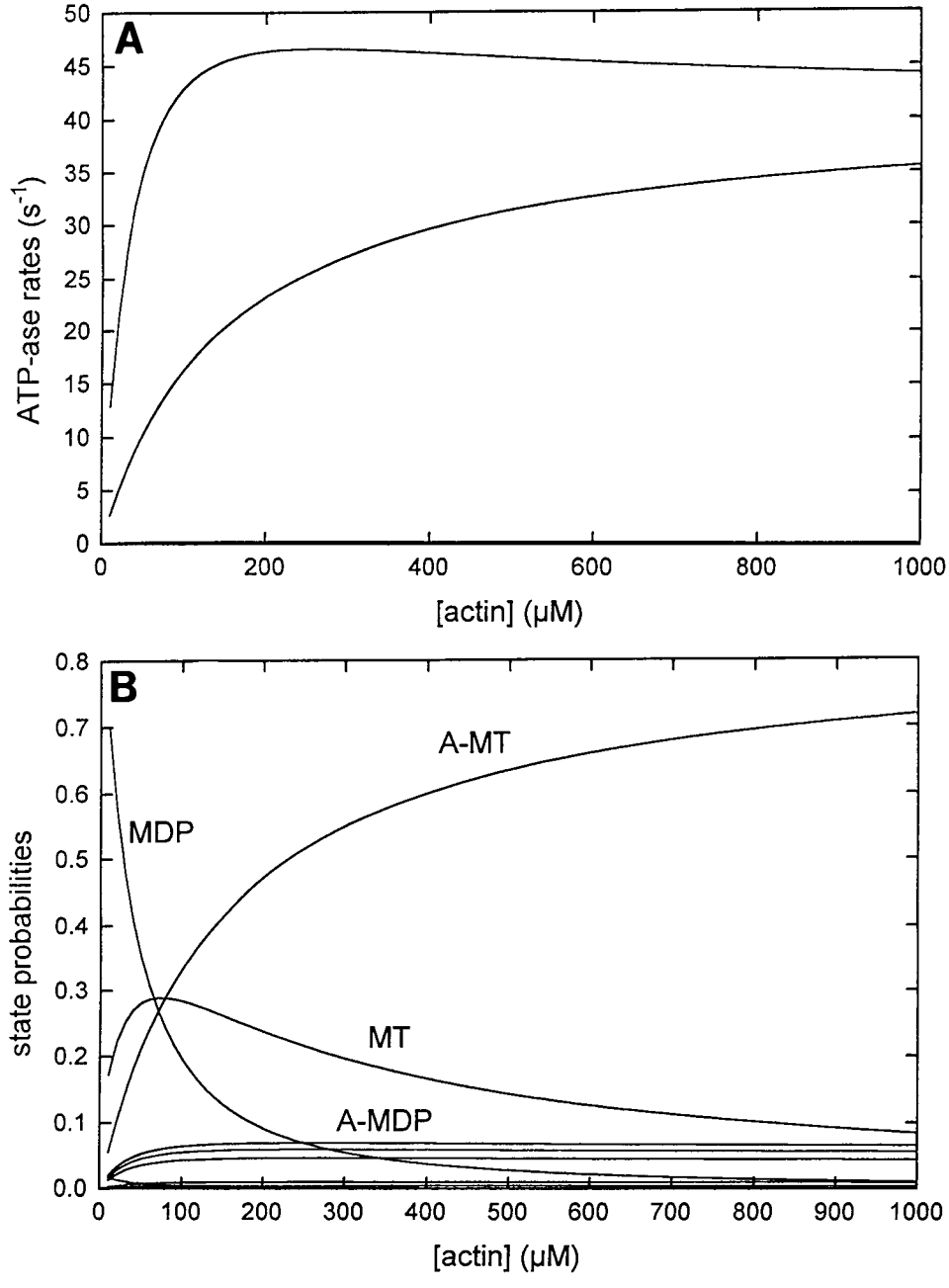

FIGURE 4 Behavior of the 3G model in solution as a function of actin concentration, showing (*A*) net ATP turnover rate and the contribution from attached heads (upper and lower traces) and (*B*) state occupation probabilities. The second-order actin-binding rates of MDP and MT in Table 1 (companion paper) were reduced by a factor of 100 to mimic conditions in low-ionic-strength solutions.

the contribution from attached states (the rotated-state contribution is again almost zero). The net rate of hydrolysis shows a maximum near 0.2-mM actin and a slow fall at higher concentrations. Fig. 4 *B* shows how the state populations develop. The initial rise in the rate is due to actin binding competing with the hydrolysis rate of free MT and is determined by the ratio of k_1 to k_H (Appendix. Eq. A2). In this region the 10:1 equilibrium admixture of MT and MDP states is rapidly replaced by a steady-state ratio near unity and produced by small amounts of actin. The fall in ATPase rate at high actin levels is due to the formation of A-MT, which partially diverts the hydrolysis path from detached to attached states. The drop is a measure of the difference in the intrinsic rates of hydrolysis $k_H^{(0)} = 100\ s^{-1}$ and $k_H^{(1)} = 50\ s^{-1}$ used in the calculation. Such a drop is also seen experimentally.

STEADY SHORTENING AND LENGTHENING

If muscle is allowed to shorten at a rate v per half-sarcomere, the steady-state tension is a decreasing and roughly hyperbolic function of v, apparently passing through zero at a value $v_0 \sim 2$–4 μm/s. The ATPase rate first increases with v, at first rapidly and then slowly, possibly saturating or reaching a maximum at speeds below but comparable with v_0 (Homsher et al., 1981; Kushmerick and Davies, 1969; Rall et al., 1976). The highest values reached may be 2–4 times the isometric rate. It is assumed that the cross-bridge mechanism has reached a steady state in these measurements. In extension, tension rises sharply with extension velocity ($-v$) and may exhibit a maximum (the "give" point of Katz (1939)) before falling. However, the height and velocity of this maximum are very dependent on muscle type and possibly on other factors. Lombardi and Piazessi (1990 a,b) have found that, in frog muscle at 5°C, tension rises to a maximum of $2.0T_0$ at a rather low extension speed and drops only slightly at much higher speeds, Harry et al. (1990) see similar behavior in rabbit psoas muscle, where the tension rises to $1.2T_0$ and then stays constant out to extension speeds of $2v_0$. In extension, the rate of ATPase quickly falls below the isometric value (Hill and Howarth, 1959).

In the context of the present model, computed solutions clearly show that not all this behavior can be reproduced by a model with a purely elastic cross-bridge element. The tension-velocity curve for shortening and the ATPase rate in extension are reasonably robust characteristics of many sliding filament models and are well simulated by the present model without modification. The unloaded contraction velocity is controlled by the extent to which tension-generating A.MD states can be dissociated from actin before they are carried into regions of negative strain, which is achieved by a high rate $k_D^{(2)}$ of unblocked ADP release. Lowering $k_D^{(2)}$ from 800 to 100 s^{-1} produces a similar fall in unloaded velocity and almost eliminates curvature in the tension-velocity function; the same effect is produced by an order-of-magnitude decrease in ATP level. Increasing the amount of strain blocking Δ_D also decreases v_0 slightly but raises isometric tension by boosting the A.MD population at positive strains. Increasing the throw distance also increases tension. There is a marginal increase in v_0 when actin-binding rates are raised by a factor of 10, thus stabilizing a near-isometric distribution of attached states in the presence of rapid motion. The value used for MDP binding is at the limit expected for a diffusion-controlled reaction. The steady-state ATPase falls with extension velocity as A.MD states are dragged into the region $x > x_*$, where they move to the attached position and are prevented from cycling.

The behavior of tension in extension cannot be reproduced by the tightly coupled form of the model; tension continues to rise steeply with extension speed, and this survives all reasonable changes in rate constants and structural parameters. Tightly coupled models also tend to produce insufficient ATPase inhibition at high speeds of shortening. Limits to elastic behavior can be viewed as one way of forcing myosin heads to detach from actin at large strains. The effects of elastic limits that modify the operation of the cross-bridge cycle are now considered for each phenomenon in turn. Strain blocking of the phosphate release step is also investigated as a means of inhibiting the ATPase rate of rapidly shortening muscle.

Steady extension

In steadily extending muscle the ADP release/ATP binding pathway to detachment is virtually inoperative, as most tension-bearing heads are swept into strain regions where they backrotate to the 90° state. Any model that requires this process before detachment will produce a severe rise in tension with extension velocity $|v|$ unless backrotation can occur fast enough. This process is rate limited by phosphate binding to the A.MD state, which must occur first. With a phosphate dissociation constant of 1 M this is impossible at all but the highest phosphate levels, even with a 1000-s^{-1} release rate. At 10 mM Pi and speeds of 2 μm/s tension-generating heads are swept through a distance of 200 nm on average before backrotation, so a new approach is needed to explain the very modest speed-independent increase observed in some fibers. In this context, Lombardi and Piazessi (1990a) suggested that tension-generating states may be forcibly detached at large positive strain.

In the present model an upper limit d_+ of 16.5 nm (three units) for elastic behavior can produce the desired reduction in tension at high $|v|$ by forcing dissociation from all rotated states according to Eq. 5 of the companion paper. Fig. 5 *A* shows the tension-velocity curves for $v < 0$ (extension). The forcing rate k_3 was 5000 s^{-1} for all rotated states, and the enhancement factors were $\beta_1 = \beta_2 = 100$. For $v < -50$ units/s the tension is generated almost entirely by A-MD states formed by forced dissociation from A.MD when $x > d_+ - 2h = 1$ and is carried by extension to x values above $b/2$ and into the next set of actin sites, entering at $x = -b/2$.

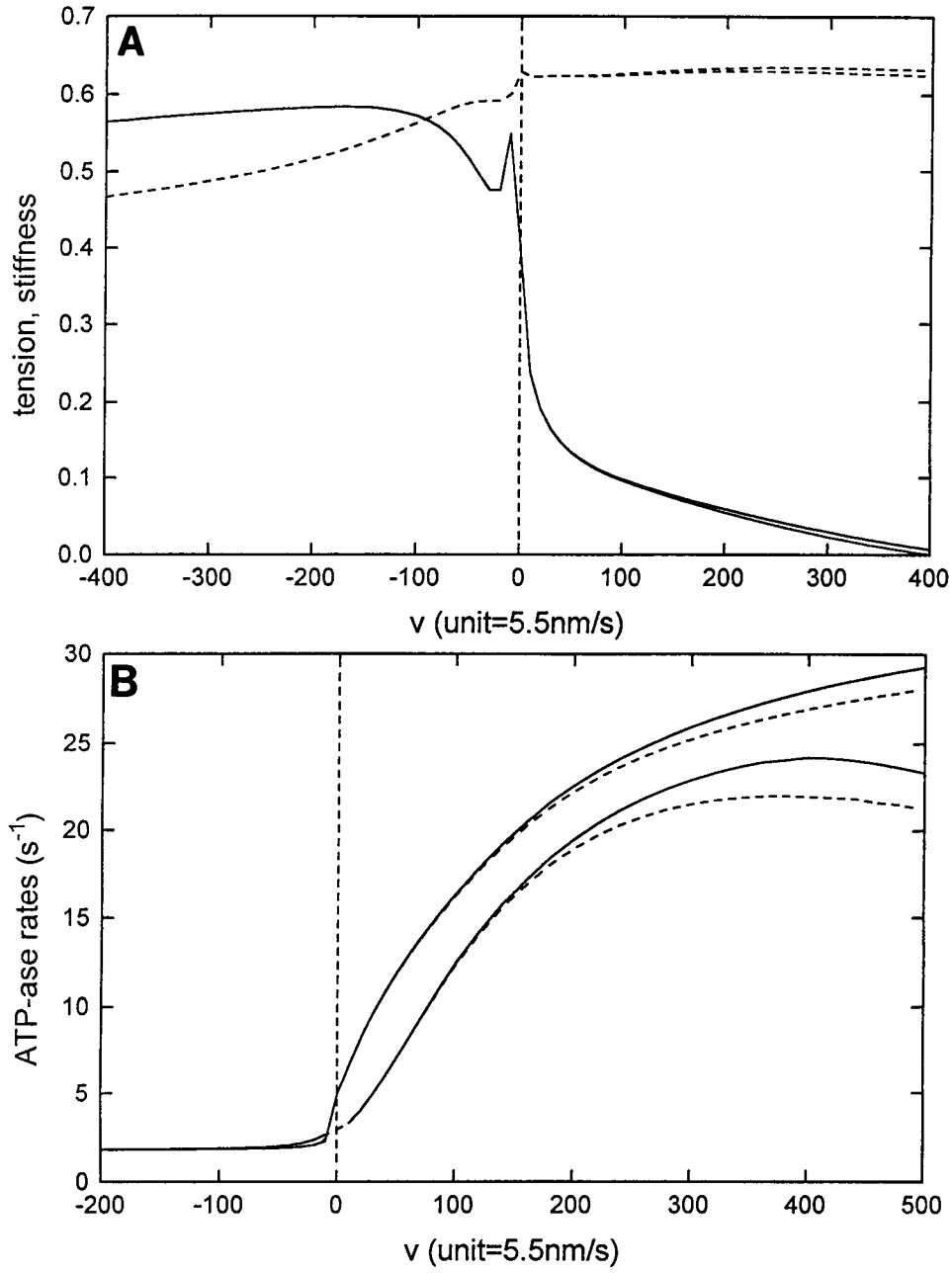

FIGURE 5 Steady-state shortening and extension behavior versus shortening velocity v per half-sarcomere and three actin sites/head unless stated otherwise. (*A*) Tension (——) and stiffness (- - - - -) curves, with and without strain dependence of phosphate release. Forced detachment at $d_+ = 16.5$ nm (three units) dramatically reduces tension in extension ($v < 0$), but $d_- = -11$ nm (−2) has no effect on tension in shortening. (*B*) ATPase rates/head for three actin sites per head (top curves) and one site (bottom curves), showing extra inhibition caused by strain-blocked phosphate release at negative strains (dashed curves, $\Delta_P = 0.7$).

This is shown in Fig. 6 *A*, where the A-MD state dominates over its binding range from below $x = 0$ to $x = d_+ = 3$, where it too is forced to detach. The probability of this state in its binding range is set by the binding rate $k_1^{(D)}$, which is the other critical parameter determining tension behavior in extension. The height of the tension plateau (here $\sim 1.5T_0$) is determined mainly by the upper elastic limit, whereas the rate of dissociation of A-MD from actin controls the subsequent decline in tension at higher extension speeds. This was verified by a series of calculations with binding rates in the range $2–6 \times 10^5$ M^{-1} s^{-1} at a fixed affinity $K_1^{(D)}$ (Table 1 of the companion paper).

Forced detachment at $d_+ = 15$ nm in the 3G model is essentially the mechanism proposed by Lombardi and Piazessi (1990a), because the upper elastic limit raises the Gibbs energy of bound states to $+oo$ and makes detachment irreversible. Their states A1 and D2 are identified as A-MD and MD, but in the 3G model A-MD is not on the main pathway. The present model predicts the rapid increase in tension observed at small extension speeds, which is produced by rotated tension-generating states just as if the upper elastic limit were absent. The subsequent decline seen in Fig. 5 *A* before the rise at larger negative v is the first consequence of forced detachment and is not a computing artifact even though numerical accuracy is at a premium at low velocities. It would not be observed in any experiment in which sarcomere lengths were not individually controlled, because individual sarcomere lengths/velocities are

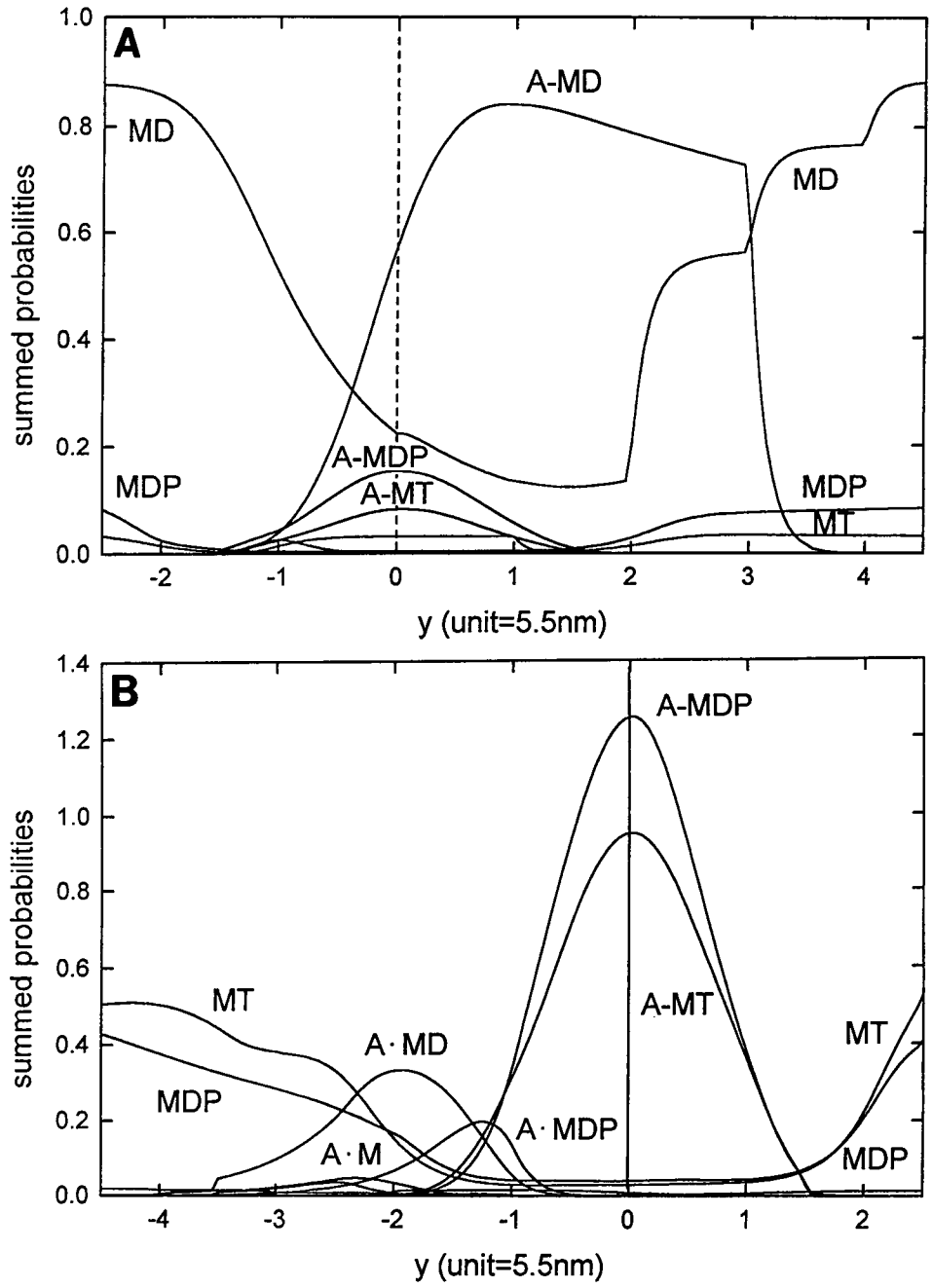

FIGURE 6 State probabilities versus strain at high velocities. (*A*) Rapid extension ($v = -500$ units/s) and forced detachment at $d_+ = 3.0$, showing A-MD (attached) as the dominant bound state and detachments to M.D occurring at $y = d_+ + l$ ($l = -1, 0, 1$) for the three actin sites used. (*B*) Unloaded shortening ($v = 450$ units/s), showing that the ratio of bound ATP to ATP has increased sevenfold over that for isometric conditions (Fig. 1). Note that bound states on different actin sites l are collated at fixed strain $y = x + l$.

determined by their common tension and the velocity for a given tension is tri-valued in the range of tensions between the extrema. Of the three possible velocity solutions for a given tension the outer two are stable and the middle one unstable, because its tension-velocity slope is negative. The same considerations may produce popping of sarcomeres at high extension speeds if the calculated tension for a single sarcomere decreases with speed (Morgan, 1990; Harry et al., 1990). Alternatively, forced detachment may occur progressively over a range of strains near 15 nm; an abrupt elastic element is computationally convenient but not necessarily realistic for polymeric structures.

Strain blocking of phosphate release is not an issue for extending muscle, as it would occur at strains less than the lowest value at which attached states form.

Steady shortening

In shortening, the tension-velocity curve is little affected either by forced detachment at any reasonable negative strain or by strain blocking of phosphate release. The results obtained were independent of forced detachment at any value of d_- below -2 units (-11 nm), which corresponds to $x + lc < d_- - 2h = -4$ units, with $h = 1$. Forced

detachment at any less negative value of d_- is to be avoided, because under isometric conditions it destroys rotated states that generate tension. This is a consequence of any model with two types of bound state with different tension capacities, provided that rotated states can be reached only via the attached ones. Forced detachment at any strain below −11 nm has little effect if the rates of unblocked ADP and phosphate release are $\approx 1000\ s^{-1}$, because the lifetime of the A.MD state is insufficient to carry it through to x values below $d_- - 2h$ where detachment is obligatory. The two curves shown in Fig. 5 *A* were obtained with and without strain-blocked phosphate release with a displacement barrier of 0.7 unit.

If ADP release and/or phosphate release rates are lowered substantially below $1000\ s^{-1}$ the unloaded contraction velocity is reduced by prolonging the lifetime of negatively strained A.MD states, and this cannot be reversed by forcing detachment at any reasonable value of $|d_-|$ (above 11 nm) because a wide region of negatively strained R states would be preserved. In fact, the ADP release rate is a major determinant of the unloaded contraction velocity, as suggested by Siemankowski et al. (1985).

The steady-state ATP turnover rate (Fig. 5 *B*) at high shortening velocities is also unaffected by forced detachment at strains below −11 nm, and for the same reason. The top curve in this figure shows less ATPase inhibition than do the experimental results, which show a plateau (and perhaps a maximum at $v \sim 0.6v_0$) of approximately four times the isometric rate (Kushmerick and Davies, 1969). In view of the preceding discussion, forced detachment in this model is not a likely mechanism for sufficient inhibition of ATPase rate in rapidly shortening muscle, at least for fast fibers. Such inhibition can certainly be achieved by forced detachment at $d_- = -1$ unit (−5.5 nm), but such detachment removes tension-generating isometric states. However, these arguments assume a throw distance of 11 nm.

Strain blocking of phosphate release is a better means of inhibiting ATPase for fast fibers, but the effect is modest. The upper dashed curve in Fig. 5 *B* was generated with a displacement barrier of 0.7 unit (3.85 nm), which puts the upper limit for strain blocking at $x = -1.65$ (Eq. 4b of the companion paper). With three actin sites per head the turnover rate at the unloaded contraction velocity ($v = 432$) is still too high. However, ATPase turnover is also sensitive to the number of allowed actin sites. With only one allowed site (lower curves of Fig. 5 *B*), strain blocking of phosphate release does reduce the turnover rate sufficiently and creates a maximum. The same effect can be achieved by lowering the rate of phosphate release to $600\ s^{-1}$. However, strain-blocked phosphate release produces a smaller drop in unloaded shortening speed and is therefore preferred as a way of minimizing ATP turnover at $v = v_0$.

In this model, excessive ATP turnover at high speeds of shortening can be traced to attached states. Calculations of the separate ATP cleavage rates from detached, attached, and rotated states show that the attached contribution increases steadily with shortening speed, whereas the detached contribution is almost velocity independent above $0.5v_0$. There is no contribution from rotated states. It is tempting to speculate that ATP cleavage from A-MT is absent in muscle fibers, but Fig. 4 *A* and the data that it models show that this is certainly not the case in solution.

Probability distributions for $v = v_0$ are shown in Fig. 6 *B* for $d_- = -2$ and no strain blocking of phosphate release. An unexpected feature is that the dominant attached states are a nearly equal mixture of A-MDP and A-MT, whereas in isometric muscle the former predominate (Fig. 1) by a factor of 10, the equilibrium constant for ATP hydrolysis on detached myosin. Thus high-speed shortening actually loads ATP into the cross-bridges: MT states formed at large negative strains by ATP-induced dissociation from actin are swept through $x = -b/2$ and onto the next set of actin sites down the thin filament starting at $x = b/2$. At large shortening speeds there is insufficient time for them to hydrolyze ATP before they are presented for binding, which is reflected in the high probability of MT states relative to MDP at each end of the allowed strain range in Fig. 6 *B*. At $v_0 = 430 \times 5.5$ nm/s they are moved by 24 nm on average before being hydrolyzed, comparable with the distance between nearest actin sites on adjacent turns of the actin double helix ($38.5 - 2 \times 5.5$ nm). At high velocities this process takes over from strain-blocked ADP release as the rate-limiting step for ATP turnover but is still insufficient to account for the observed rates at high speed. In fast fibers the best possibility seems to be a combination of strain-blocked phosphate release and a reduced number of available actin sites (one) per turn of the actin helix.

Note that calculations were made by shifting the range of x values from (−3.5, 3.5) to $(x_m - 7, x_m)$, where $x_m = 4.5$ in extension and $x_m = 2.5$ for shortening, to localize all bound states within the range chosen. Bound-state distributions were independent of the choice of x_m, provided that this condition was satisfied.

DISCUSSION

We have shown that many steady-state properties of striated muscle can be deduced from the kinetics of the solution proteins described by the 3G model by using the sliding filament model in conjunction with simple structural postulates and the transition-state theory. However, different models based on the same solution kinetics can be devised, and some parts of the 3G cycle are not well characterized or are still controversial. Structurally distinct alternatives to this model were canvassed at the end of the companion paper. Here we review what changes to the model, if any, are indicated by its steady-state predictions.

The logarithmic law for the phosphate dependence of isometric tension is important for two reasons. The explanation of this law (verified computationally in Fig. 2 *G* for [*P*] above 1 mM) in terms of moving the boundary separating the strain distributions of A and R states requires the main A-to-R transition to take place *before* phosphate is

released. This enables Pi release to be incorporated formally within the A-to-R transition (Eq. 9b, companion paper). The same association is implicit in the calculations of Pate and Cooke (1989). If Pi were released in the attached state, the release would function kinetically as a postbinding event, and the dependence on Pi level would be absorbed into K_1, not into K_2, giving a square-root dependence of x_+ on ln[P] and a weaker (and nonlinear) tension variation with ln[P]. Secondly, this logarithmic law would be changed by the use of nonstereospecific A states, because the A-to-R equilibrium constant would also acquire the strain dependence previously associated with S1 binding, at least over the range of strain-free binding angles.

The phosphate dependence of transient properties remains difficult to fit within any simple biochemical model of the cross-bridge cycle. Several different transient experiments (Dantzig et al., 1992; Kawai and Halvorson, 1991; Fortune et al., 1991; Millar and Homsher, 1990) show a phosphate-dependent rate of relaxation of the order of 100 s^{-1}, with a M-M constant of 10 mM with respect to phosphate. This behavior can probably be produced by an ad hoc modification of the 3G model with $\tilde{K}_P^{(2)}$ reduced from 1 to 0.01 M. However, this change destroys the predicted phosphate dependence of isometric tension and unloaded contraction velocity (Fig. 2 *G* and *I*), which agree with experiment. It appears that a collision state for phosphate binding should be introduced to allow phosphate at the 10-mM level to increase the net rate of escape from A.MD without changing the overall equilibrium constant. Kawai et al. (1987) also concluded that excess phosphate was having effects not included in the traditional cross-bridge cycle, resulting in more oscillatory work.

The tightly coupled form of the model is moderately successful in inhibiting ATP turnover at high speeds of shortening; a maximum ATPase rate at speeds below v_0 can be achieved with blocked Pi release at negative strains and only one actin site per half-pitch of F-actin (Fig. 5 *B*). Modeling indicates that the speed of the maximum as a fraction of v_0 is relatively independent of v_0 itself, which is controlled by the strain-free ADP release rate. The uncertainty of experimental data at large v reduces the significance of this test, but the maximum does appear to be very broad. Models with forced detachment at negative strains are certainly much better at inhibiting ATPase at high shortening speeds (Cooke et al., 1994), but this degree of inhibition is not reflected in the data. ATPase inhibition in their model may also be due to the slow ADP isomerization step, which pushes long-lived A.MDP states into regions of negative strain not realized in the present model with ADP release at 800s^{-1}, and to the absence of a binding rate for compressed heads. Thus numerical predictions for ATPase rates versus velocity do not clearly favor one model or the other, and the issue could perhaps be resolved from solution-kinetic studies to establish whether a second A.MD state lies on the main pathway.

In the present model, forced detachment at compressions of 11 nm or more has almost no effect on v_0 or ATPase rates under rapid shortening, because the rates of phosphate and ADP release were kept high to achieve high values of v_0. ATPase inhibition at high v can be achieved by forcing detachment at -5 nm, but only at the cost of destroying isometric tension-bearing states. This could be avoided if there were different lower elastic limits for attached and rotated states, which, if true, would have implications for the location of elastic elements in the S1–S2 structure. Models with variable angles of S1 attachment to actin would give the same effect if strain-free binding were allowed over a range of ±5.5 nm or more, and a smaller throw distance would help. Thus there are several ways in which forced irreversible detachment at large strains can be implemented, with different results.

Measurements of ATPase rates (or the rate of heat production) are restricted to the time of shortening over the 0.2-μm plateau of the tension–length curve. This is only 100 ms at v = 2 (μm/s)/half-sarcomere, which is comparable with the duration of the rate-limiting step (ATP hydrolysis) at these speeds. Hence the ATPase rate may not have reached a steady–state at high shortening speeds, particularly as the rate of heat production is known to be in excess of ATPase rates measured in the first stages of unloaded shortening (Homsher et al., 1981). That result may be related to our prediction that the proportion of unhydrolyzed ATP on myosin (both free and bound to actin) is much higher in freely shortening than in isometric muscle. The time required for a steady state to be established from the onset of unloaded shortening will be investigated in a later paper.

At large positive strains, forced detachment is essential to explain the mechanical properties of extending muscle. The behavior observed by Lombardi and Piazessi (1990a,b) arises naturally from the 3G model, which predicts that at most extension speeds the attached A-MD state is the main tension carrier. This state arises from forced detachment of the normal carrier state A.MD. The isomerization rate from A-MD to A.MD observed in solution (Geeves, 1991) is too low to allow the latter to be regenerated in the presence of forced detachment, and this prediction may be testable.

The role of the second S1 head in heavy meromyosin needs to be explored quantitatively, and the predictions of all models using independent S1 heads should be treated as provisional. It seems likely that one S1 stays detached while the other head binds and cycles, but in rigor it is known that both heads are attached (Reedy et al., 1965). Thus comparisons of tension and stiffness in the active and rigor states can lead to different estimates for stiffness per head. With three actin sites available per head in the active state, our predicted binding fraction of 60% is in fact only 30% if the inactive S1 is included in the total. Rigor tensions, and those at very low concentrations of ATP, are therefore likely to be twice what is predicted from this model, but note that steady-state predictions at the low-ATP end of Figs. 2 *A–C* are unlikely to be realized experimentally because very slow actin-binding rates are involved. Kinetic correlations be-

tween the two heads of HMM might also lower the ratio of maximum ATPase rate in shortening to the isometric rate, as the ratio predicted by single-S1 cross-bridge theories (usually ~6) is probably too high.

These tests of the strain-dependent 3G model suggest that its basic assumptions, particularly the existence of orientationally well-defined attached and rotated states of acto S1 for every nucleotide state, are viable. The observed linear dependence of isometric tension on ln[phosphate] arises only from models with attached and rotated tension-bearing states. No extra states are required for the description of tension at high extension speeds once forced detachment is allowed, because the model automatically predicts that tension is then carried by attached A-MD states. The model predicts that an explanation of tension behavior under rapid extension requires forced detachments at large positive strains. Strain-dependent phosphate release seems to be a possible explanation for the inhibition of the ATPase under rapid shortening, particularly if the number of available actin sites/head is reduced at high velocities through factors not included in the present model. For fast fibers, forced detachment at negative strains is not a means of inhibiting ATPase in this model with a throw distance of 11 nm.

APPENDIX

Analysis of a reduced four-state model for isometric properties

To isolate the factors that populate tension-generating states and the way in which they are affected by nucleotide levels, a simplified version of the cross-bridge cycle can be used in which the head rotation and phosphate release steps are both in rapid equilibrium. The ATP hydrolysis pathway on attached states is omitted, as are states M, MD, A-M, and A-MD, which are not populated under isometric conditions and millimolar levels of ATP. Fig. 7 shows the simplified cycle. The exit fractions $\gamma_A(x)$ and $\gamma_D(x)$ from the A-MDP and A.MD ends of the composite state II are given by

$$\gamma_A(x) = \frac{1}{1 + K_2(x)(1 + K_P)}, \qquad \gamma_D(x) = \frac{K_2(x)K_P}{1 + K_2(x)(1 + K_P)}. \tag{A1}$$

Superscript labels are omitted, and $K_P = \tilde{K}_P/[P]$, $K_D = \tilde{K}_D/[D]$, $k_T = \tilde{k}_T[T]$, where a tilde indicates a second-order constant.

The steady-state flux $J(x)$ through this cycle for a given strain x is

$$\frac{1}{J(x)} = \frac{1}{k_H} + \left(1 + \frac{1}{K_H}\right)\frac{1}{k_1(x)} + \left[1 + \left(1 + \frac{1}{K_H}\right)\frac{\gamma_A(x)}{K_1(x)}\right]\frac{1}{\gamma_D(x)k_D(x)} + \left\{1 + \frac{1}{\gamma_D(x)K_D}\left[1 + \left(1 + \frac{1}{K_H}\right)\frac{\gamma_A(x)}{K_1(x)}\right]\right\}\frac{1}{k_T(x)}, \tag{A2}$$

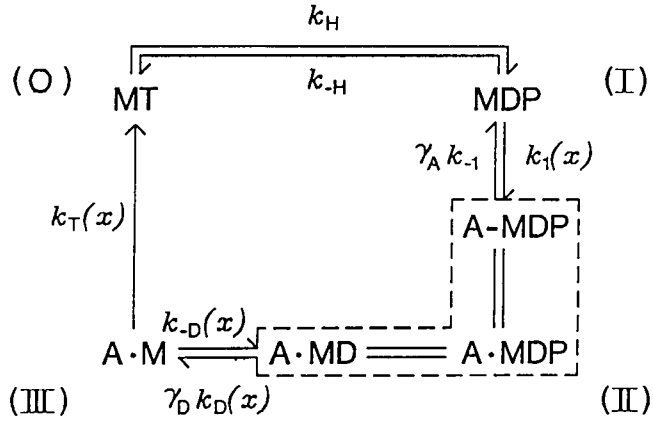

FIGURE 7 Reduced cross-bridge cycle for analyzing isometric properties. ATP hydrolysis paths on attached and rotated states are removed, ATP binding to S1 and its dissociation from actin are treated as a single irreversible step, and the head rotation and phosphate release steps are both treated as in rapid equilibrium. The exit fractions from the combined state II are given in Eq. A1.

from which the bound-state probabilities are obtained as

$$p_{III}(x) = \frac{J(x)}{k_T(x)}, \qquad p_{II}(x) = \left(1 + \frac{k_{-D}(x)}{k_T(x)}\right)\frac{J(x)}{\gamma_D(x)k_D(x)}. \tag{A3}$$

Isometric tension is given by the integral

$$T_0 = \frac{k}{b}\int [x\gamma_A(x) + (x + 2h)(1 - \gamma_A(x))]\, p_{II}(x)dx + \frac{k}{b}\int (x + 2h)p_{III}(x)dx, \tag{A4}$$

which is useful for a qualitative analysis of the effects of nucleotide levels on tension. It is sufficient to use an approximate evaluation of Eq. A4 that assumes that all bound states are attached states for $x > x_*$ (Eq. 9b of the companion paper) and rotated otherwise: inasmuch as $K_2(x) = \exp(-2\alpha(x - x_*)/h)$ this is valid only for very large values of α. Then

$$x > x_*: \qquad p_{II}(x) = \frac{K_1(x)}{1 + \frac{1}{K_H} + K_1(x)}, \qquad p_{III}(x) = 0; \tag{A5}$$

also $J(x) = \gamma_D(x) = 0$. There is no cycling, and P_{II} is independent of nucleotides or phosphates. Hence nucleotides affect only tension from the following region:

$$x < x_*: \qquad T_0 \text{ contribution} = \frac{1}{b}\int_{-b/2}^{x_*} (x + 2h) \times (p_{II}(x) + p_{III}(x))dx, \tag{A6}$$

which is Eq. A4 with $\gamma_A(x) = 0$. In this region

$$p_{II}(x) + p_{III}(x) = \frac{\frac{1}{\tilde{k}_T(x)[T]} + \left(1 + \frac{C[D]}{[T]}\right)\frac{1}{k_D(x)}}{\frac{1}{k_H} + \left(1 + \frac{1}{K_H}\right)\frac{1}{k_1(x)} + \frac{1}{\tilde{k}_T(x)[T]} + \left(1 + \frac{C[D]}{[T]}\right)\frac{1}{k_D(x)}}, \quad \text{(A7)}$$

where $C = \tilde{k}_D/\tilde{k}_T$ (Eq. 4) and the dependences on nucleotide concentrations $[T]$ and $[D]$ are shown. The energy barriers for D release and T binding are assumed equal, which permits cancellation of some strain-dependent factors.

The left-hand edge x_- of the population of rotated states can now be estimated by setting Eq. A7 equal to 0.5, giving the equation

$$\frac{1}{k_H} + \left(1 + \frac{1}{K_H}\right)\frac{1}{k_1(x)} = \frac{1}{\tilde{k}_T(x)[T]} + \left(1 + \frac{C[D]}{[T]}\right)\frac{1}{k_D(x)} \quad \text{(A8)}$$

for x_-. The left-hand side of Eq. A8 is a decreasing function of x, and the right-hand side an increasing function for $x < x$. Hence x_- is shifted downward as the ratio $[D]/[T]$ increases.

The peak value of $p_{II} + p_{III}$ occurs at a larger value of x, at which $k_1(x)$ is larger and not rate limiting in Eq. A7. Then the strain dependences of D release and T binding cancel almost everywhere, and

$$(p_{II} + p_{III})_{max} = \frac{1 + \left(1 + \frac{C[D]}{[T]}\right)\frac{\tilde{k}_T[T]}{k_D}}{\frac{\tilde{k}_T(x)[T]}{k_H} + 1 + \left(1 + \frac{C[D]}{[T]}\right)\frac{\tilde{k}_T[T]}{k_D}}, \quad \text{(A9)}$$

where the x value is chosen to give the maximum. Without knowing exactly what this value is, we can calculate strain-dependent M-M constants for this quantity (and hence for tension) with respect to ATP and ADP levels. These are

$$K_T(x) = \frac{C[D] + \frac{k_D}{\tilde{k}_T}}{1 + \frac{k_D(x)}{k_H}},$$

$$K_D(x) = \tilde{K}_D\left(1 + \frac{\tilde{k}_T(x)[T]}{k_H}\right) + \frac{[T]}{C} \geq \frac{[T]}{C} + \tilde{K}_D. \quad \text{(A10)}$$

Fractional shifts in the peak population of states II + III caused by moving the ATP level down through K_T and the ADP level up through K_D are estimated at

$$\frac{k_D(x)}{k_H} \quad ([T]\text{ fraction}), \quad \text{(A11a)}$$

$$\frac{k_D(x)\tilde{k}_T[T]}{k_H(\tilde{k}_T[T] + k_D)} \quad ([D]\text{ fraction}), \quad \text{(A11b)}$$

where $x \approx -1$ for a maximum in Eq. A10. Hence the effects of changing nucleotide concentrations are felt in tension only if Δ_D is small enough not to strain block ADP release completely at this value of x.

We wish to thank many colleagues for their encouragement while this study was in progress. Prof. Roger Goody and Dr. Malcolm Irving for helpful discussions, and Prof. Freddie Gutfreund for reading the manuscripts. Also, we are grateful to members of the computing section for assistance and to C. Berse and F. Dräger for expert preparation of figures.

REFERENCES

Cooke, R., and W. Bialek. 1979. Contraction of glycerinated muscle fibers as a function of ATP concentration. *Biophys. J.* 28:241–258.

Cooke, R., and E. Pate. 1985. The effects of ADP and phosphate on the contraction of muscle fibers. *Biophys. J.* 48:789–798.

Cooke, R., H. White, and E. Pate. 1994. A model of the release of myosin heads from actin in rapidly contracting muscle fibers. *Biophys. J.* 66: 778–788.

Dantzig, J. A., Y. E. Goldman, N. C. Millar, J. Lacktis, and E. Homsher. 1992. Reversal of the cross-bridge force-generating transition by photogeneration of phosphate in rabbit psoas muscle fibres. *J. Physiol. (London).* 451:247–278.

Dantzig, J. A., M. G. Hibberd, D. R. Trentham, and Y. E. Goldman. 1991. Cross-bridge kinetics in the presence of MgADP investigated by photolysis of caged ATP in rabbit psoas muscle fibers. *J. Physiol. (London).* 432:639–680.

Edman, K. A. P. 1979. The velocity of unloaded shortening and its relation to sarcomere length and isometric force in vertebrate striated muscle. *J. Physiol. (London).* 291:143–159.

Ferenczi, M. A., Y. E. Goldman, and R. M. Simmons. 1984a. The dependence of force and shortening velocity on substrate concentration in skinned muscle fibers from Rana temporaria. *J. Physiol. (London).* 350:519–543.

Ferenczi, M. A., E. Homsher, and D. R. Trentham. 1984b. The kinetics of magnesium adenosine triphosphate cleavage in skinned muscle fibres of the rabbit. *J. Physiol. (London).* 352:575–599.

Ferenczi, M. A., R. M. Simmons, and J. A. Sleep. 1982. General considerations of crossbridge models in relation to the dependence on MgATP concentration of mechanical parameters of skinned fibers from frog muscle. *In* Basic Biology of Muscles: A Comparative Approach. B. M. Twarog, R. J. C. Levine, and M. M. Dewey, Editors, Raven Press, New York.

Finer, J. T., R. M. Simmons, and J. A. Spudich. 1994. Single myosin molecule mechanics: piconewton forces and nanometric steps. *Nature (London).* 368:113–119.

Fortune, N. S., M. A. Geeves, and K. W. Ranatunga. 1991. Tension responses to rapid pressure release in glycerinated rabbit muscle fibres: effects of hydrostatic pressure. *J. Physiol. (London).* 407:53–75.

Geeves, M. A. 1991. The dynamics of actin and myosin association and the crossbridge model of muscle contraction. *Biochem. J.* 274:1–14.

Geeves, M. A. 1992. The actomyosin ATP-ase: a two-state system. *Phil Trans. R. Soc. B.* 336:63–71.

Geeves, M. A., R. S. Goody, and H. Gutfreund. 1984. Kinetics of acto–S1 interaction as a guide to a model for the crossbridge cycle. *J. Muscle Res. Cell Motil.* 5:351–361.

Harry, J. D., A. W. Ward, N. C. Heglund, D. L. Morgan, and T. A. McMahon. 1990. Cross-bridge cycling theories cannot explain high-speed lengthening behavior in frog muscle. *Biophys. J.* 57:201–208.

Hermann, C., C. Lionne, F. Travers, and T. Barman. 1994. Correlation of actoS1, myofibrillar and muscle fiber ATP-ases. *Biochemistry.* 33: 4148–4154.

Hill, A. V., and J. V. Howarth. 1959. The reversal of chemical reactions in contracting muscle during an applied stretch. *Proc. R. Soc. (London) Ser. B.* 151:169–193.

Homsher, E., M. Irving, and A. Wallner. 1981. High-energy phosphate metabolism and energy liberation associated with rapid shortening in frog skeletal muscle. *J. Physiol. (London).* 321:423–436.

Huxley, A. F., and R. M. Simmons. 1971. Proposed mechanism of force generation in striated muscle. *Nature (London).* 233:533–538.

Katz, B. 1939. The relation between force and speed in muscle contraction. *J. Physiol. (London).* 96:45–64.

Kawai, M., K. Guth, K. Winnikes, C. Haist, and J. C. Ruegg. 1987. The effect of inorganic phosphate on the ATP hydrolysis rate and the tension transients in chemically skinned rabbit psoas fibres. *Pflugers Arch.* 498:1–9.

Kawai, M., and H. R. Halvorson. 1991. Two-step mechanism of phosphate release and the mechanism of force generation in chemically skinned fibers of rabbit psoas muscle. *Biophys. J.* 59:329–342.

Kushmerick, M. J., and R. E. Davies. 1969. The chemical energy of muscle contraction II. The chemistry, efficiency and power of maximally working sartorius muscles. *Proc. R. Soc. London Ser. B.* 174:315–353.

Lombardi, V., and G. Piazessi. 1990a. The contractile response during steady lengthening of stimulated frog muscle fibres. *J. Physiol. (London).* 443:141–171.

Lombardi, V., and G. Piazessi. 1990b. Force response in steady lengthening of active single muscle fibres. *In* Muscular Contraction. R. M. Simmons, editor. Cambridge University Press, Cambridge, UK. pp. 237–255.

Millar, N. C., and E. Homsher. 1990. The effect of phosphate and calcium on force generation in glycerinated rabbit skeletal muscle fibers. *J. Biol. Chem.* 265, 20234–20240.

Millar, N. C., and E. Homsher. 1992. Kinetics of force generation and phosphate release in skinned rabbit soleus muscle fibers. *Am. J. Physiol.* 262:C11239–C1245.

Morgan, D. L. 1990. New insights into the behavior of muscle during active lengthening. *Biophys. J.* 57:209–222.

Pate, E., and R. Cooke. 1989. A model of cross-bridge action: the effects of ATP, ADP and Pi. *J. Muscle Res. Cell Motil.* 10:181–196.

Rall, J. A., E. Homsher, A. Wallner, and W. F. H. M. Mommaerts. 1976. A temporal dissociation of energy liberation and high energy phosphate splitting during shortening in frog skeletal muscles. *J. Gen. Physiol.* 68:13–27.

Reedy, M. K., K. C. Holmes, and R. T. Tregear. 1965. Induced changes in orientation of the crossbridges in glycerinated insect flight muscle. *Nature (London).* 207:1276–1280.

Siemankowski, R. F., M. O. Wiseman, and H. White. 1985. ADP dissociation from actomyosin subfragment 1 is sufficiently slow to limit the unloaded shortening velocity in vertebrate muscle. *Proc. Natl. Acad. Sci. USA.* 82:658–662.

Smith, D. A., and M. E. Geeves. 1995. Strain-dependent cross-bridge cycle for muscle. *Biophys. J.* 69. In press.

Stein, L. A., R. P. Schwarz, P. B. Chock, and E. Eisenberg. 1979. Mechanism of actomyosin triphosphatase. Evidence that adenosine 5′-triphosphatase hydrolysis can occur without dissociation of the actomyosin complex. *Biochemistry* 18:3895–3909.

Stein, L. A., P. B. Chock, and E. Eisenberg. 1981. Mechanism of the actomyosin ATP-ase: effect of actin on the ATP hydrolysis step. *Proc. Natl. Acad. Sci. USA.* 78:1346–1350.